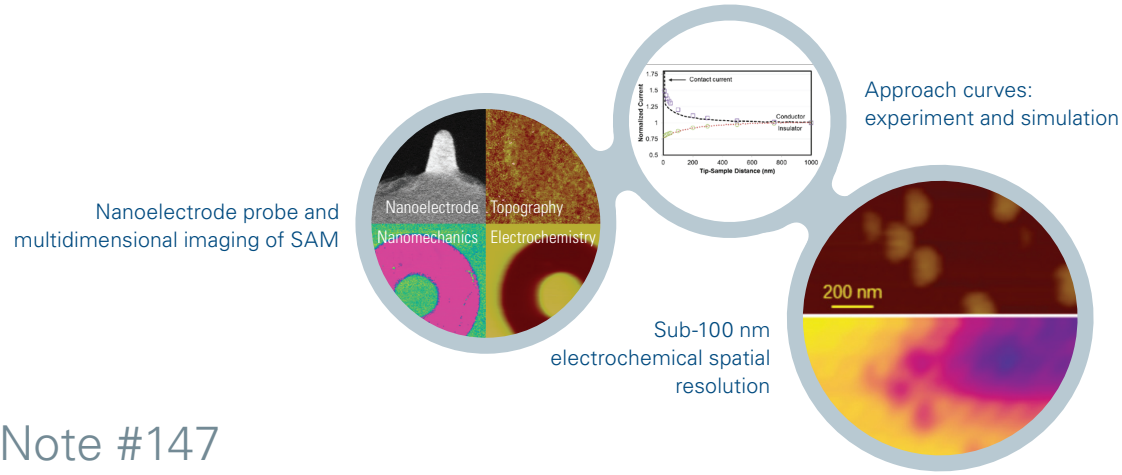

Application Note #147

An Introduction to AFM-Based Scanning Electrochemical Microscopy: PeakForce SECM

This application note discusses PeakForce SECM™, the world's first complete commercial solution for AFM-based scanning electrochemical microscopy. With a spatial resolution less than 100 nm, PeakForce SECM uniquely provides simultaneous capture of topographical, electrochemical, electrical, and mechanical maps with nanoscale lateral resolution. This mode is made possible by proprietary batch-fabricated SECM nanoelectrode probes that exhibit a characteristic dimension of approximately 50 nm. The pairing of these nanoelectrode probes with high-bandwidth electronics enables high-quality nanoelectrical imaging in liquid. A number of applications are detailed that showcase how the PeakForce SECM capability is helping enable multidisciplinary research in a wide arena of markets.

Introduction

Electrochemistry deals with the interplay between electrical and chemical energy, where electrons drive chemical reactions or chemical changes to move electric charges.[1] Many electrochemistry applications impact our daily lives, from chemical manufacturing to frontier R&D activities in energy research, biological systems, materials development, and surface protection.[2-5] However, macroscopic electrochemical behavior is an average of the heterogeneous reactivity over an electrode surface. This may include different active sites, crystal-facet-dependent properties, or surface defects.[6] Reactivity variation is also a result of the heterogeneity in structural, mechanical, electrical, and/or electrochemical properties over the electrode surface.[7,8] Therefore, for today's highly multidisciplinary research, in situ, localized techniques capable of simultaneously capturing both nanoscale multidimensional information and electrochemistry are highly desired.[9,10]

Scanning electrochemical microscopy (SECM) is the most popular and established approach for local electrochemical studies at micro- and nanoscales.[11-13] In classic SECM, an ultramicroelectrode (UME, 5–25 µm) positioned in close proximity to the sample is scanned across the surface. The nature and properties of the sample area underneath the probe influence the electrochemical processes at the electrode tip. By capturing the current and/or potential response of the tip during scanning, the variation of electrochemical properties is imaged. However, it is very challenging to achieve sub-µm resolution with classic SECM. Additionally, the popular constant height and constant current modes suffer from convolution issues between topography and electrochemistry since the tip current depends on both the surface properties and the tip-sample distance. Traditional SECM typically can obtain no more than electrochemical and topographical information, which is insufficient for a complex system, such as batteries.[13]

Atomic force microscopy (AFM) is known for its high-spatial-resolution imaging capability. Since the invention of SECM in 1980s,[14] there have been constant efforts to implement an UME as an AFM probe for integrated AFM-SECM imaging to decouple topographic and electrochemical information.[15] Meanwhile, parallel efforts have been made to convert an AFM probe into a nanoelectrode to achieve sub-µm or even sub-100 nm resolution.[16-21] However, after about two decades of development,[19,22-24] it remains a great challenge to realize the batch production of stable, reliable, and cost-effective nanoelectrode probes with a characteristic dimension of sub-100 nm.

AFM-SECM generally relies on either traditional contact mode or tapping mode for imaging. However, contact mode is not suitable for soft and fragile samples due to the high imaging and shear forces. For tapping mode, the imaging force is reduced and shear force is minimized, but as the method relies on a mechanical resonance, the mode is sensitive to the working environment of the probe. In 2009, Bruker developed PeakForce Tapping® mode,[25] which preserves the advantages of both conventional contact and tapping modes while avoiding the disadvantages from both. In this mode, the probe is modulated sinusoidally off-resonance, at a low frequency (typically 1–2 kHz) with a small amplitude (typically 5–100 nm). Additionally, cantilever tuning is not required, which is convenient for liquid imaging. PeakForce Tapping performs a triggered force curve at every tapping cycle as the feedback signal is the maximum force, or peak force, between the tip and the sample. Real-time analysis of these force curves allows for simultaneous, quantitative imaging of mechanical properties at a normal AFM scan rate (Bruker's PeakForce QNM® mode).[26] Utilizing sinusoidal modulation, the tip velocity is nearly zero as it approaches the surface. This allows for stable, precise force control, ultralow imaging force (<50 pN), and automatic image optimization. PeakForce QNM imaging has been successfully integrated with a variety of advanced AFM modes to further enhance their capabilities, including electrical mapping (PeakForce TUNA™),[27] surface spreading resistance microscopy (PeakForce SSRM™), Kelvin probe force microscopy (PeakForce KPFM™),[28] and scanning microwave impedance microscopy (PeakForce sMIM™).[29]

Bruker has also developed batch-fabricated, high-quality, robust PeakForce SECM probes with a characteristic tip dimension of approximately 50 nm. With these probes, PeakForce SECM scanning is obtained, which simultaneously provides nanoscale topographical, electrical, and quantitative mechanical maps, along with sub-100-nm-resolution electrochemical images. When used with high-bandwidth electronics, it also provides unique capabilities for high-quality nanoelectrical imaging in liquid.

A Pioneering Nanoelectrode Probe

Bruker spent considerable time and effort to develop a nanoelectrode probe that could enable consistent SECM capability. The resulting SECM nanoelectrode probe was fabricated through a wafer-based MEMS approach to guarantee high consistency in probe fabrication. The pre-mounted PeakForce SECM probe is shown in Figure 1a.[30] Components of this probe assembly have been rigorously tested for chemical compatibility, showing ≤1% change in mass over 5 days of immersion in solutions/solvent, as listed in Table 1. These solvent/solutions include pH 1 and pH 13 aqueous solutions, solvents frequently used in non-aqueous electrochemistry, and liquid generally used in Li-ion battery systems. The mounted nanoelectrode probe has a much larger size than a regular AFM probe (11.7 x 6.1 x 3.7 mm versus 3.4 x 1.6 x 0.3 mm), and the glass packaging has handling grooves. Both features provide increased safety and ease of use. The rectangular cantilever is shown in Figure 1b. A 11-µm-wide Pt conductive path runs between the tip and the base and provides electrical conductivity (Figure 1c). This approach has been employed previously to minimize the possible formation of pin holes in the passivation layer on the Pt surface.[24, 31] The apex of the tip, as shown in Figure 1d, has a Pt coated area of ~50 nm in diameter and ~200 nm tip height. Other than this small electrochemically active region, the probe is fully insulated by a layer of SiO_2 to limit leakage, which is crucial for all nanoelectrochemical and nanoelectrical measurements in liquid.

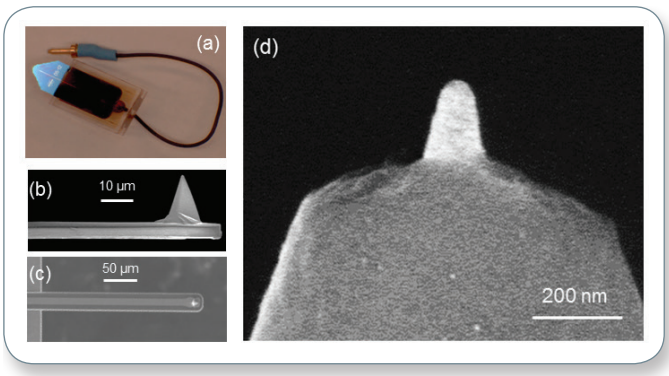

Figure 1. (a) Pre-mounted PeakForce SECM probe; (b) SEM side view image of the cantilever; (c) SEM top view image of the cantilever showing the 15-µm-wide Pt conductive path; (d) SEM image revealing exposed Pt-coated tip apex with ~50 nm end-tip diameter and ~200 nm tip height (adapted from Nellist et al., *Nanotechnology,* 2017, 28(9), 095711, IOP Publishing[30]).

Table 1. Solvents and solutions for chemical compatibility Test

Aqueous solution (0.1 M)	NaOH, KOH, HCl, H_2SO_4,HNO_3, and H_2O_2
Organic solvents	Acetonitrile, 1-methyl-2-pyrrolidinone, ethyl acetate, toluene, methanol, ethanol, and acetone
Solvents/solutions for Li-ion batteries	Diethyl carbonate, dimethyl carbonate, ethyl methyl carbonate; 1 M $LiPF_6$ in ethylene carbonate : dimethyl carbonate (1:1 in volume)

PeakForce SECM Hardware and Operation

PeakForce SECM hardware includes a PeakForce SECM probe holder, a protective Kalrez® boot, and a strain-released module with resistance selector (0, 1, and 10 MΩ) to limit the maximum current flow, as shown in Figure 2.[32] The module avoids direct electrical connection to the probe, which generally causes mechanical noises. The 10 MΩ current-limiting resistor is generally selected. Although this 10 MΩ resistor limits the current to <100 nA, the SECM probe can handle currents in excess of 1 µA in PeakForce Tapping mode, and 600 nA when in constant contact with a conductive substrate.[30] This hardware operates in conjunction with the standard Bruker EC-AFM kit with temperature control from ambient to 65˚C.

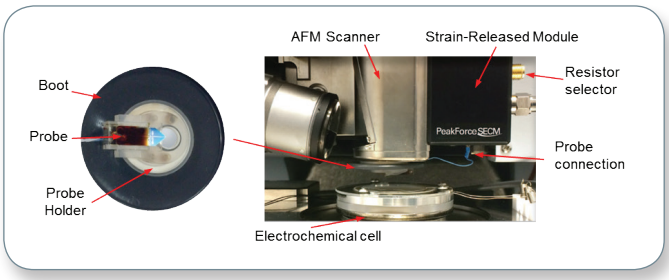

Figure 2. PeakForce SECM accessories with a pre-mounted nanoelectrode probe loaded. (adapted from Huang, Z. *et al.*[32]).

PeakForce SECM integrates PeakForce QNM® mode with AFM-SECM functions as shown in Figure 3. Both the probe and the sample are working electrodes and share the same reference and counter electrodes. During SECM measurement, the probe and the sample are generally biased at different potentials to enable different chemical reactions. For example, the probe reduces the $[Ru(NH_3)_6]^{3+}$ to $[Ru(NH_3)_6]^{2+}$ at -350 to -500 mV versus a Ag/AgCl or a Ag/AgCl-quasi reference electrode (AgQRE), while the sample is biased at 0 to -100 mV for $[Ru(NH_3)_6]^{3+}$ regeneration. For imaging, PeakForce SECM can utilize the advantages of LiftMode™, as illustrated in Figure 3b. During the main scan, PeakForce QNM imaging is performed. In addition to topography and mechanical properties, the contact current is also imaged. During the lift scan, the probe follows the stored topographic profile while maintaining a constant tip-sample distance defined by the lift height. While the probe is lifted, electrochemical information is captured. In this way, PeakForce SECM allows for simultaneously mapping multi-dimensional properties, including topography, mechanics, conductivity, and electrochemistry. This is a versatile capability that has never been achieved before.

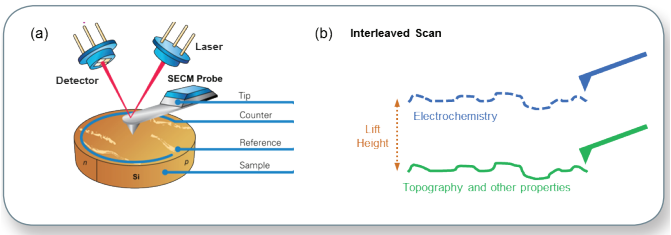

Figure 3. (a) Schematic illustration of a PeakForce SECM system showing the major mechanical and electronic components; and (b) an illustration of interleaved scanning mode.

COMSOL Simulation

Figure 4 shows the COMSOL simulation of the concentration profile when the probe is exposed to a $[Ru(NH_3)_6]^{2+/3+}$ solution, and performs a reduction reaction.[33] This type of nanoelectrode features a three-dimensional, radial, convergent diffusive transport, which leads to a steady-state diffusion layer (Figure 4a). This layer is highly compact. The normalized concentration profile from the electrode surface following the center axis (Figure 4b) shows 60% recovery of the $[Ru(NH_3)_6]^{3+}$ concentration at 50 nm away from the electrode surface. Since electrochemical imaging is sensed by the perturbation to the diffusion layer, such a compact layer is required for sub-100 nm spatial resolution. The steady-state diffusive transport also results in a steady-state diffusion-limited current. Simulation performed for a probe in 10 mM $[Ru(NH_3)_6]^{3+}$ and 0.1 M KCl solution yield a diffusion-limited current of 720 pA, consistent with experimental results (0.75 ± 0.45 nA).[30] The time for establishing such a steady state decreases with the probe dimension and are only <10 µs for a nanoelectrode.[34] The steady-state probing current, rapid response to external perturbations, and small characteristic dimension with a tight diffusion layer are the three premises for high-resolution electrochemical imaging in PeakForce SECM.

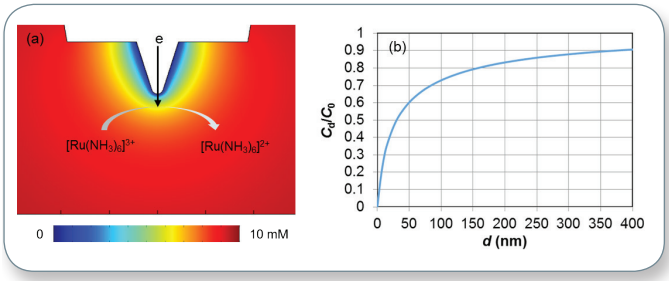

Figure 4. (a) COMSOL simulation of the $[Ru(NH_3)_6]^{3+}$ concentration profile; (b) a normalized concentration profile from the electrode surface following the center axis. C_d is the $[Ru(NH_3)_6]^{3+}$ concentration at a distance, d, from the electrode surface, and C_0 is the bulk $[Ru(NH_3)_6]^{3+}$ concentration. Simulation conditions are 10 mM $[Ru(NH_3)_6]^{3+}$ and 10 mM $[Ru(NH_3)_6]^{2+}$ in the bulk, and the probe is 1 mm away from an insulating substrate.

Electrochemical Performance

Cyclic voltammetry (CV) and amperometry

Figure 5a overlays the 1st, 25th and 50th cycles of a nanoelectrode probe from 50 continuous cyclic scans. No performance degradation is observed. The sigmoidal shape of the CV curves are expected for a nanoelectrode due to the radial diffusion process. The capactive charging current is ~5 pA at 20 mV/s scanning rate. The probe was cleaned for a subsequent amperometric test as shown in Figure 5b, which also demonstrates stable performance of the nanoelectrode probe for more than 2 hours. The inset in Figure 5b also shows the current drift of <2 pA and over 30 min sub-pA noise level in this measurement.[30]

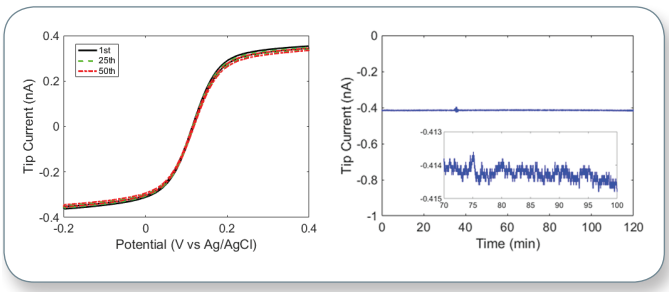

Figure 5. (a) The 1st, 25th and 50th CVs selected from 50 continuous scans at a scan rate of 20 mV/s; and (b) 2-hour amperometric test at -0.1 V vs Ag/AgCl. The inset is magnification from 70 to 120 min. Solution: 5 mM $[Fe(CN)_6]^{4-}$, 5 mM$[Fe(CN)_6]^{3-}$ and 0.1 M KNO_3.

Approach curves

Figure 6 shows typical approach curves captured from an insulating (red dotted) and a conductive (blue dashed) surface, respectively. These curves are normalized to the tip current at a tip-sample distance of 1 µm. On an insulator, the diffusion of $[Ru(NH_3)_6]^{3+}$ to the electrode surface is increasingly blocked as the tip-sample distance decreases. The ~25% current reduction on an insulating surface is consistent with the COMSOL simulation (open circles). While on a conducting surface biased for oxidation of $[Ru(NH_3)_6]^{2+}$ to regenerate $[Ru(NH_3)_6]^{3+}$, increasing the local concentration of $[Ru(NH_3)_6]^{3+}$ at the tip. This positive feedback competes with the negative blocking effect, and thus, results in current enhancement (black dashed). In this case, a >25% current enhancement is obtained, which is consistent with the simulation (open squares). Figure 6 also demonstrates that the current enhancement/reduction primarily occurs at <100 nm tip-sample distance. This is consistent with the thickness of the diffusion layer in Figure 4a and such a high-spatial sensitivity is desired for high-resolution electrochemical imaging.

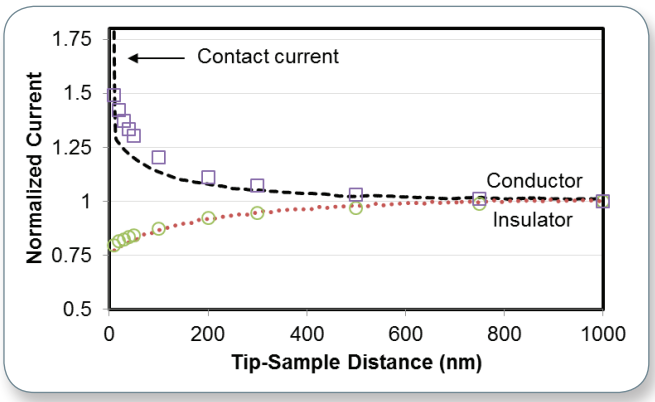

Figure 6. Approach curves captured on insulating (red dotted) and conducting (black dashed) surfaces. The tip and the substrate were biased at 0 and -0.5 V vs AgQRE, respectively. The solution was 10 mM $[Ru(NH_3)_6]^{3+}$ with 0.1 M KCl supporting electrolyte. Symbol plots are COMSOL-simulated results. These results are normalized at the tip-sample distance of 1 µm.

PeakForce SECM Imaging

A sample with a 50-nm-thick patterned silicon nitride layer deposited onto an Au substrate was tested using PeakForce SECM. The tip voltage was -0.4 V versus Ag/AgCl for reducing $[Ru(NH_3)_6]^{3+}$, while the sample potential was -0.1 V for the regeneration of $[Ru(NH_3)_6]^{3+}$. As shown in Figure 7, when the tip is in contact with the Au surface during the PeakForce Tapping cycle, the 300 mV difference between the tip and the sample leads to a current upon contact of tip and sample. During the lift scan, the electrochemical current clearly differentiates between the Au and nitride regions, as shown in Figure 7b. As expected, the contact current is much larger than the noncontact electrochemical current.[32]

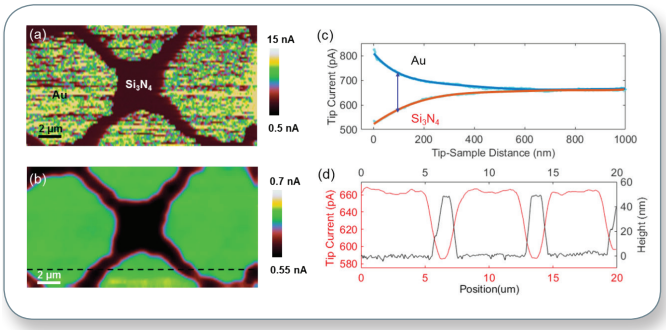

Figure 7. PeakForce SECM measurement of an electrode with a 50-nm-thick patterned silicon nitride layer deposited on an Au substrate: (a) Map of current response from the PeakForce Tapping scan; (b) electrochemical current map at a lift height of 100 nm (dashed line indicates location for cross-sectional analysis); (c) approach curves on Au and nitride regions plotted with respect to the probe movement, respectively; (d) line profiles of tip current during the lift scan (solid-red: left y-axis) and surface topography (dashed-green: right y-axis). Solution, 10 mM $[Ru(NH_3)_6]^{3+}$ and 0.1 M KCl (figures a and b were adopted from Huang, Z. *et al.*[32]).

Approach curves were captured on both the Au and nitride regions, and compared in Figure 7c. These two curves are plotted with respect to the tip-sample distance. When the probe approaches the nitride surface, the diffusion of $[Ru(NH_3)_6]^{3+}$ toward the probe is increasingly blocked, resulting in current reduction. Conversely, for the Au surface, the regeneration of $[Ru(NH_3)_6]^{3+}$ on the surface increases the current, outperforming the blocking effect. When the tip is ~100 nm away from the sample surface, the current difference between the nitride and the Au is ~100 pA, corresponding to the current contrast in Figure 7b. To correlate the electrochemical activity with the surface topography, the line profiles at the same location for both the topographical height and the electrochemical current were compared (Figure 7d). The variation in the electrochemical current tracks the surface features with a sub-micron resolution. The current over the nitride is ~90 pA lower than that on the Au surface, although the nitride surface is topographically 50 nm higher than the Au substrate. This indicates that the electrochemical information is well decoupled from the topographic features. The ~90 pA difference is also consistent with that shown on the approaching curves in Figure 7c.[32]

Conductivity Measurements in Liquid

The SECM probe allows one to perform high-quality electrical measurements in liquids. The tip is fully insulated except for its apex. The coating greatly reduces both stray capacitance due to the small electrically exposed area and stray current from electrochemical reactions of chemical impurities. For conductivity measurement with PeakForce Tapping, the tip intermittently contacts the surface for ~100 µs so that electronics with a bandwidth of about 15 kHz is required. The PeakForce tunneling AFM (PeakForce TUNA™) hardware provides this capability, while maintaining low noise (<70 fA). In this way, nanoelectrical imaging in liquid with sub-pA sensitivity and with simultaneous nanomechanical imaging is possible.

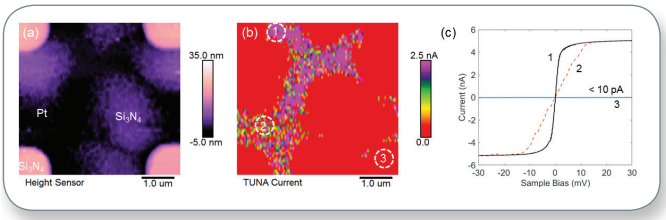

Figure 8. PeakForce TUNA measurement of a Pt surface partially covered by Si_3N_4: (a) topography; (b) TUNA currents at a sample bias of 10 mV; and (c) point-and-shoot I-V spectroscopy at selected locations in 8b (adapted from Nellist et al., *Nanotechnology*, 2017, 28(9), 095711, IOP Publishing[30]).

Figure 8 shows a PeakForce TUNA measurement using a nanoelectrode probe in dimethyl carbonate solvent performed in an Ar-filled glovebox with <1 ppm O_2 and H_2O contents. Figure 8a is the surface topography showing four Si_3N_4 corners. Among the Si_3N_4 islands is a Pt substrate partially covered by other Si_3N_4. The exposed Pt area can be seen on Figure 8a and more clearly resolved in the conductivity map in Figure 8b. PeakForce TUNA is also capable of point-and-shoot measurements to pinpoint the location of interest for current-voltage (I-V) spectroscopy as shown in Figure 8c. The plots are numerically labeled corresponding to locations indicated in Figure 8b. The blue solid line is a plot of current captured when the tip was landed on the nitride island. The capacitive current was ~5 pA and is barely seen on the figure. The plateau on plot #1 and #2 are the saturation current at the 1 nA/V sensitivity setting. Figure 8c illustrates that the background current is negligible for the measurement on the Pt surface. Locations with higher conductivities show I-V behaviors with larger slopes.[30]

PeakForce SECM Application Examples

Au-SiO_2 nanomesh electrode

Like many crucial components in such optoelectronic devices as photovoltaic cells and solar fuels devices, Au nanomesh is a stretchable, foldable, transparent conducting electrode.[35,36] In addition, electrode materials such as Au and Pt are excellent catalysts for fuel-generating photoelectrochemical reactions, such as solar-driven hydrogen evolution.[37]

Figure 9a shows an Au nanomesh electrode supported on a SiO_2 substrate prepared by nanosphere lithography.[38] This mesh has through-hole patterns of a hexagonal lattice with a period of 1 µm. The hole diameter is 750 nm, leaving an inter-hole spacing of 250 nm. The depth of the hole is about 80 nm and fabrication imperfections result in exposed SiO_2 inside the holes of ~400 x 500 nm. The electrochemical image in Figure 9b shows the expected variation of the tip current across the nanomesh electrode. The top Au surface has enhanced tip current due to the positive feedback,

while current reduction from a surface contaminant is also shown. Inside the hole, the tip current is reduced by the blocking effect resulting from both the hole feature and the exposed inactive SiO_2 substrate. As shown in Figure 9b, the sizes of the low current features (brown dots) are consistent with the ~400 x 500 nm elliptical regions inside the holes. Figure 9c is a cross-sectional analysis comparing the topographic and electrochemical line profiles at the same location, as indicated by the dashed lines in Figure 9a and 9b. The tip current profile tightly tracks the height variation of the sample, indicating a <100 nm spatial resolution for electrochemical imaging using the PeakForce SECM technique.[30]

As shown on the approach curves in Figures 6 and 7c, and confirmed here, the difference in tip current between conductor and insulator decreases with increasing tip-sample distances and is most sensitive when the tip-sample distance is comparable to the thickness of the diffusion layer. Figure 9d shows the tip current variations across a hole feature of the nanomesh electrode captured at varied lift heights while the same line position was scanned multiple times. The lift heights were gradually increased from 50 nm to 400 nm and then decreased back to 75 nm. From the electrochemical map, color contrast among different regions is clearly seen at a lift height of 50 nm while the contrast gradually disappears for increasing lift heights. At tip-sample separations of 400 nm no significant contrast is observed. COMSOL simulations in Figure 4a predict the $[Ru(NH_3)_6]^{3+}$ concentration 400 nm away from the surface to be >90% of the bulk concentration. Therefore, a much lower spatial sensitivity is expected. The tip current contrast is also clearly illustrated by the cross-sectional analysis shown in Figure 9e. On the Au region, the tip current decreases as the lift height increases. With rising tip-sample separation the current enhancing effect due to redox-cycling of the Ru-complex is reduced until the diffusion-limited current in bulk solution is reached. Conversely, on the SiO_2 regions, a larger tip-sample separation reduces the blocking of the Ru-complex diffusion to the tip electrode, resulting in an increased diffusion-limited current. As a consequence of these two effects on Au and SiO_2, respectively, the tip current contrast diminishes with increasing lift height.

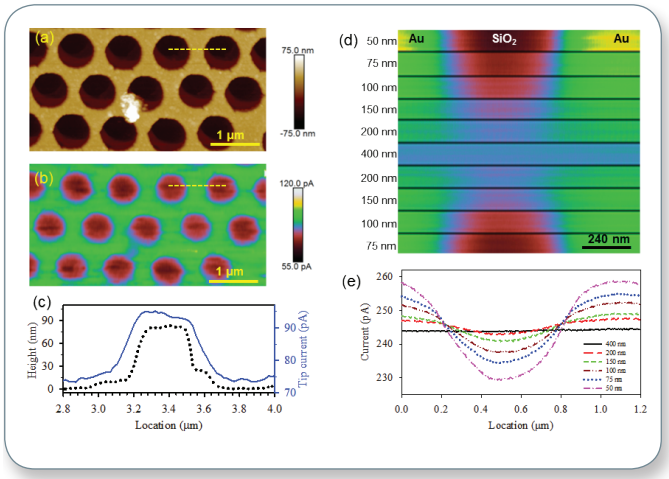

Figure 9. PeakForce SECM images of a Au-SiO_2 nanomesh electrode prepared by nanosphere lithography: (a) topography of the Au pattern on the SiO_2 substrate; (b) electrochemical map captured in the lift scan, while following the sample topography at a separation of 75 nm; (c) line profiles of both the topographic height and electrochemical current at the same location, labeled by the yellow dashed lines in (a) and (b); (d) tip current at sequentially varied lift heights as indicated in the image (tip and sample potentials were -0.1 V and -0.4 V vs Ag/AgCl, respectively); (e) the tip current contrast is clearly illustrated by cross-sectional analysis (adapted from Nellist et al., *Nanotechnology,* 2017, 28(9), 095711, IOP Publishing[30]).

Charge transfer dynamics

By capturing and studying the approach curves, SECM is well suited for quantifying the local interfacial charge transfer dynamics.[14,39] Figure 10a shows a Si_3N_4 patterned sample on a Pt substrate. The nitride pattern has 2 x 2 µm squares in a simple square lattice with 3 µm period. The gap between two nitride squares is 1 µm. The etching of nitride to achieve this pattern was not complete, resulting in limited exposed areas of the Pt substrate. Figure 10b is the map of contact current during the main scan of PeakForce SECM imaging. The Pt grid can be seen clearly by the higher current versus the nitride squares. In addition, the incomplete etching is confirmed by the inhomogeneous contact current over the Pt region. During the lift scan, the electrochemical current is captured, which can be directly correlated with the conductivity map. As shown in Figure 10c, regions that have higher conductivity are also more active in electrochemistry. Approach curves captured from locations of different activities are compared in Figure 10d. All these plots are normalized to the current at 1 µm tip-sample distance. The black curve was captured on the nitride square, which shows 22% of current reduction at the nitride surface. Others were captured on the Pt grid regions where the positive feedback enhances the tip current, resulting in less current reduction on the approach curves than the one from the nitride surface. The shapes of these approach curves depend on the surface electrochemical activities. When on a conductive surface, a

contact current can be achieved as well as shown by the cyan and red plots. Assisted with simulation, quantitative information about interfacial charge transfer dynamics can be derived from this set of approach curves.

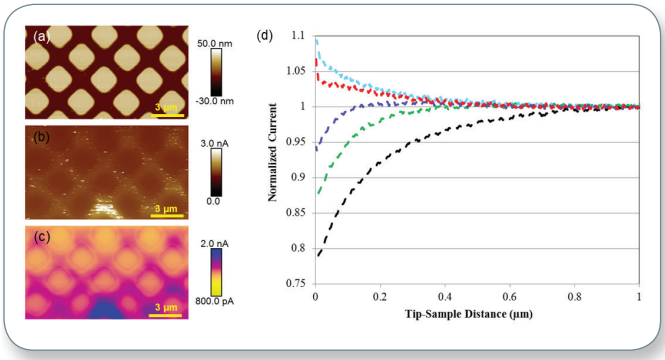

Figure 10. (a) A Si_3N_4 patterned sample on Pt substrate; (b) tip current during the main scan of PeakForce SECM imaging; (c) the electrochemical current map; and (d) approach curves captured from locations of different activities. All these plots are normalized to the current at 1 µm tip-sample distance. The black curve was captured on the nitride square. Others were captured on the Pt grid regions.

Self-assembled monolayers (SAM)

SAMs are used as etch resist barriers to charge transfer for electrochemistry and organic/molecular electronics, and as platforms for biological surfaces and sensors.[40] An ideal SAM should have topographical homogeneity (flatness and compactness without surface defects), controlled conductivity, mechanical stability, and chemical stability. When utilized in electrochemical sensors, its electrochemical properties should also be tailorable. PeakForce SECM meets the requirements for characterizing SAM samples to acquire quantitative, high-resolution, and multidimensional information.

In this case study, an ultra-flat gold electrode chemically patterned by micro-contact printing of CH_3-thiol SAMs was investigated. The topography in Figure 11a shows height variations smaller than 1 nm, which rules out topographic convolution on other imaged properties. However, the donut structure is clearly observable by the quantitative adhesion force signal obtained through PeakForce QNM, one of the functions in PeakForce SECM. Figure 11b demonstrates ~1 nN difference in adhesion forces between the tip-SAM and tip-Au interactions. The adhesion force is extremely sensitive to the surface chemistry as shown by defects with <100 nm width on the SAM (Figure 11b). For electrochemistry, the thiol layer acts as a non-ideal insulator that leads to a reduced interfacial charge transfer, and hence decreased electrochemical current. Figure 11c illustrates this behavior. On the thiol SAM layer the tip current is reduced by 110 pA compared to that on the bare Au-electrode.[32]

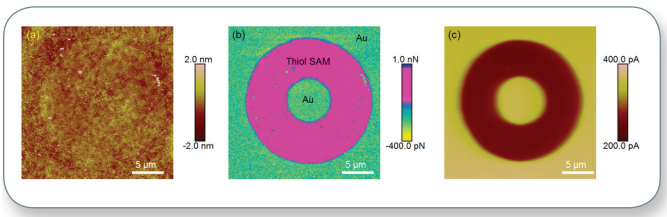

Figure 11. PeakForce SECM images of micro-contact printed CH_3-thiol self-assembled monolayer (SAM) on an Au substrate: (a) topography; (b) adhesion; and (c) electrochemical activity. Solution, 5 mM $[Ru(NH_3)_6]^{3+}$ and 0.1 M KNO_3 (adapted and modified from Huang, Z. *et al.* [32]).

Highly oriented pyrolytic graphite (HOPG)

HOPG is an important electrode or electrode material for numerous applications, such as functionalized interfaces, electrochemical sensors, and electrocatalysis. Understanding of the electrochemistry at the basal surface, the step edges, and the defects of HOPG is crucial for the rational designs of related devices. The electrochemical characteristics of HOPG have been attracting considerable attention and the study of HOPG on the nanoscale by SECM remains an active research area.[41-43] Conventionally, researchers can only achieve either topographic information by AFM or electrochemical maps by SECM. This limitation can be now overcome by PeakForce SECM.

As shown in Figure 12a, a ~600 x 900 nm defect area on the HOPG surface is observed on the height image. This defect region is 0.4 nm higher than the surrounding terrace. This defect region has a faradic current ~55 pA or 10% less than the basal area (485 pA versus 540 pA, Figure 12b). Figure 12b also shows slightly enhanced tip currents at the step edges, which is about 2–5 pA higher than the terraces.[30]

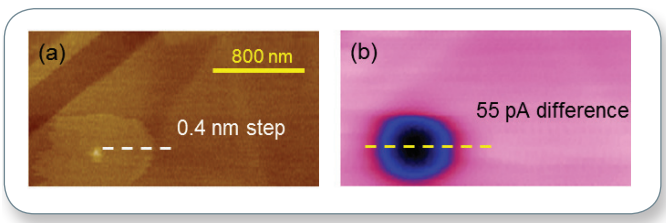

Figure 12. PeakForce SECM images of an HOPG sample: (a) topography; (b) electrochemistry (adapted from Nellist et al., *Nanotechnology*, 2017, 28(9), 095711, IOP Publishing[30]).

Nanoparticle (NP) catalysis

Today, nanoparticle catalysts deposited onto and dispersed over various supports have found applications in many fields, including chemical manufacturing, energy-related applications, and environmental remediation.[44, 45] The compositions, sizes, shapes, structures, patterns, and interfaces with the substrates are all crucial for the resulting activity, selectivity, and stability of these catalysts. The heterogeneous natures of these catalysts often possess

spatial variation down to a single-particle level at the nanoscale.[10] In addition, the electrolyte or surrounding media can also have strong impacts on performance.[46] Therefore, high-resolution in situ studies that can simultaneously achieve multi-dimensional information are highly desired.

For PeakForce SECM measurements on a Pt NP/p^+-Si electrode (Figure 13), the probe and sample are biased at -0.4 V and -0.1 versus AgQRE, respectively. A 700 pN imaging force was used to avoid moving the particles, which are loosely attached to the substrate. Figure 13a is the surface topography showing particles with different sizes (~50 to ~200 nm). For the convenience of comparison, we numerically label some representative particles and an area. Figure 13b is the tip current captured from the main scan during the SECM imaging. Figure 13c is an image of the tip current captured during the lift scan at 100 nm lift height. Both images clearly resolve the four particles, demonstrating sub-100 nm spatial resolving power of the electrochemical imaging. From these correlated maps, one can compare the surface topography, contact current, and tip faradic current among different particles in detail. As shown on the contact current in the main scan, even particles only loosely attached to the Si surface can carry a large current density (e.g., particle 3, >4 nA, or ~2.5 mA cm^{-2}). However, the interfacial conductivity is not homogeneous among particles, as shown in Figure 13b. In addition, particles 3 and 4 show similar activities, albeit with a great difference in interfacial conductivity. This suggests that the rate-limiting step is the surface electrochemical reaction. The difference in electrochemical activities can result from multiple factors, such as compositions, sizes, shapes, structures, etc. Deconvolution of these contributions remains a challenge.[10]

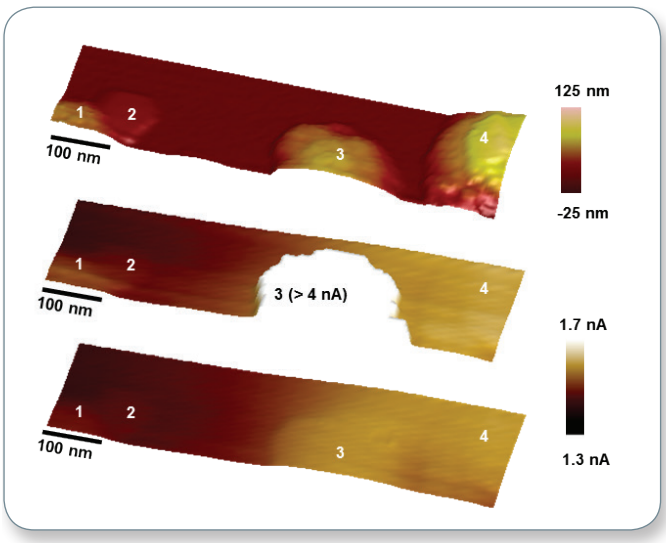

Figure 13. PeakForce SECM images of a semiconductor electrode decorated with nanoparticle catalysts; (a) topography; (b) tip current from the main scan; and (c) electrochemistry from the lift scan. The particles are numerically labelled for comparison.

Utilizing PeakForce TUNA for Semiconductor/Metal Junctions in Liquid

Correct junction behaviors (tunneling, diode-like, or Ohmic) are critical for semiconductor devices that rely on the metal-semiconductor contacts. The critical parameter for these junctions is the Schottky barrier height, which depends on the Fermi levels of both materials, and the interfacial chemistry, e.g., Fermi level pinning. Semiconductor photoelectrodes decorated with metal nanoparticle catalysts (typically Pt, Au or Ag) are generally used for light- or solar-driven decomposition of pollutants in aqueous solution, water purification to remove organic contaminants, and artificial photosynthesis. In these circumstances, the photoelectrode is exposed to the electrolyte solution, which has strong impact on interfacial energetics of the semiconductor/metal junction. This is particularly the case when nanoparticle metal catalysts are used.[47]

Figure 14 is an example of PeakForce TUNA using a nanoelectrode probe in deionized H_2O. The sample is an Au nanoelectrode array on a semiconductor substrate. When a +0.3 V sample bias was applied, the nanoelectrode dots had current responses clearly different from the surrounding oxide. The contact currents range from hundreds of pA up to few nA. To better understand the junction behaviors and sources of the current signals, the I-V characteristics of these nanoelectrodes were compared to the oxide areas in deionized H_2O, as shown in Figure 14c. For each measurement, the voltage for forward and backward ramping was cycled at 400 mV/s and both curves were plotted together. When the tip landed on an oxide region in liquid, only background capacitive charging current (grey curves) was detected. This current can be more clearly seen in the inset of Figure 14c, where it shows a charging current of ~150 pA. While on the Au dot, the I-V curves show non-linear behaviors deviating from either an Ohmic contact or a diode junction (green-red curves). The slight hysteresis of the cyclic ramping is better presented in the inset. This hysteresis results in a ~300 pA current difference between the forward and backward scans. This difference is consistent with the capacitive charging current when the tip is placed on the oxide region. Therefore, the I-V behavior of the red-green plot is a true reflection of the junction properties of the semiconductor/metal contact on the nanoelectrode. However, interestingly, this junction behavior in liquid is markedly different from that in air, where it shows typical rectifying characteristics that indicates a diode junction (blue curves).[32]

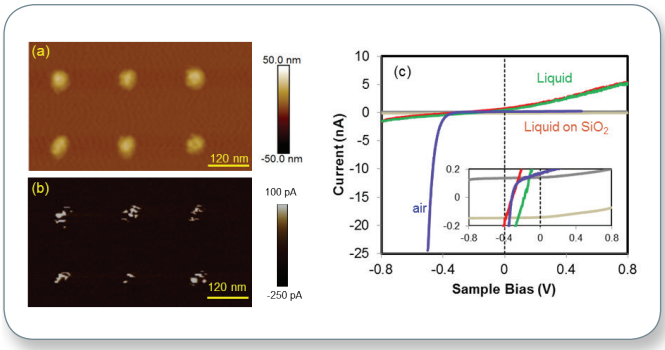

Figure 14. High-resolution PeakForce TUNA in de-ionized H_2O measurement for conductivity mapping of an Au nanoelectrode array sample: (A) topography; (B) current map at +0.3 V; and (C) comparison of I-V characteristics of the semiconductor/metal junction in air (blue) and liquid (green-red). The background current in liquid is captured by landing the probe at the oxide region (grey). Voltage ramp rates of 400 mV/s were employed. For each measurement, the voltage was cycled for both the forward and backward ramping and the curves were plotted together (adapted and modified from Huang, Z. *et al.* [32]).

Conclusion

This application note illustrates Bruker's success in batch-fabrication of high-quality, robust, and easy-to-use PeakForce SECM probes with an exposed Pt-coated tip apex having a ~200 nm height and an end tip diameter of ~50 nm. These probes are adopted for the novel PeakForce SECM mode, which integrates PeakForce QNM and conductive AFM with AFM-SECM measurements. From this mode, a complete solution for simultaneously capturing topographical, electrical, and mechanical maps with nanometer-scale and for electrochemical images with <100 nm resolution has been successfully developed. PeakForce SECM also provides capabilities for high-quality nanoelectric imaging in liquid environments. All these features were developed to meet the needs of today's highly multidisciplinary research fields, as illustrated by a variety of application examples in this work.

Acknowledgements

GP and MR acknowledge the support from the German Research Foundation (DFG) in the framework of the Collaborative Research Center (SFB 840). SWB and MRM acknowledge the support from the Department of Energy, Basic Energy Sciences, award number DE-SC0014279. CX and JJ acknowledge support from the Joint Center for Artificial Photosynthesis, a DOE Energy Innovation Hub, supported through the Office of Science of the U.S. Department of Energy under Award Number DE-SC0004993, BSB acknowledges support from NSF under the NSF Center CHE-1305124. Research was in part carried out at the Molecular Materials Research Center of the Beckman Institute of the California Institute of Technology.

References

1. Penner, R. M. and Gogotsi, Y., "The Rising and Receding Fortunes of Electrochemists," *ACS Nano* 10, 3875-76, (2016).
2. Ambrosi, A., Chua, C. K., Bonanni, A. and Pumera, M., "Electrochemistry of Graphene and Related Materials", *Chem Rev* 114, 7150-88, (2014).
3. Palecek, E. et al., "Electrochemistry of Nonconjugated Proteins and Glycoproteins. Toward Sensors for Biomedicine and Glycomics," *Chem Rev* 115, 2045-108, (2015).
4. Zhu, C. Z., Du, D., Eychmuller, A. and Lin, Y. H., "Engineering Ordered and Nonordered Porous Noble Metal Nanostructures: Synthesis, Assembly, and Their Applications in Electrochemistry," *Chem Rev* 115, 8896-943, (2015).
5. Reddington, E. et al., "Combinatorial Electrochemistry: A Highly Parallel, Optical Screening Method for Discovery of Better Electrocatalysts," *Science* 280, 1735-37, (1998).
6. Zhu, J. et al., "Direct Imaging of Highly Anisotropic Photogenerated Charge Separations on Different Facets of a Single BiVO4 Photocatalyst," *Angew Chem Int Edit* 54, 9111-14, (2015).
7. Tokranov, A., Sheldon, B. W., Li, C. Z., Minne, S. and Xiao, X. C., "In Situ Atomic Force Microscopy Study of Initial Solid Electrolyte Interphase Formation on Silicon Electrodes for Li-Ion Batteries." *ACS Appl Mater Inter* 6, 6672-86, (2014).
8. Tokranov, A., Kumar, R., Li, C., Minne, S., Xiao, X., and Sheldon, B. W., "Control and Optimization of the Electrochemical and Mechanical Properties of the Solid Electrolyte Interphase on Silicon Electrodes in Lithium Ion Batteries," *Adv. Energy Mater*, (2016).
9. Oja, S. M., Fan, Y. S., Armstrong, C. M., Defnet, P. and Zhang, B., "Nanoscale Electrochemistry Revisited," *Anal Chem* 88, 414-30, (2016).
10. Esposito, D. V. et al., "Methods of Photoelectrode Characterization with High Spatial and Temporal Resolution," *Energ Environ Sci* 8, 2863-85, (2015).
11. Zoski, C. G., "Review-Advances in Scanning Electrochemical Microscopy (SECM)," *J Electrochem Soc* 163, H3088-100, (2016).
12. Fan, F. R. F. and Bard, A. J., "Electrochemical Detection of Single Molecules," *Science* 267, 871-74, (1995).
13. Ventosa, E. and Schuhmann, W., "Scanning Electrochemical Microscopy of Li-ion Batteries," *Phys Chem Chem Phys* 17, 28441-50, (2015).

14. Bard, A. J., Fan, F. R. F., Kwak, J. and Lev, O., "Scanning Electrochemical Microscopy - Introduction and Principles," *Anal Chem* 61, 132-38, (1989).

15. Macpherson, J. V., Unwin, P. R., Hillier, A. C. and Bard, A. J., "In-Situ Imaging of Ionic Crystal Dissolution Using an Integrated Electrochemical/AFM Probe," *J Am Chem Soc* 118, 6445-52 (1996).

16. Zhu, Y. Y. and Williams, D. E., "Scanning Electrochemical Microscopic Observation of a Precursor State to Pitting Corrosion of Stainless Steel," *J Electrochem Soc* 144, L43-45, (1997).

17. Macpherson, J. V. and Unwin, P. R., "Combined Scanning Electrochemical-Atomic Force Microscopy," *Anal Chem* 72, 276-85 (2000).

18. Macpherson, J. V. and Unwin, P. R., "Noncontact Electrochemical Imaging with Combined Scanning Electrochemical Atomic Force Microscopy," *Anal Chem* 73, 550-57 (2001).

19. Akiyama, T. et al., "Insulated Conductive Probes for In Situ Experiments in Structural Biology," *Aip Conf Proc* 696, 166-71 (2003).

20. Alfonta, L. et al., "Measuring Localized Redox Enzyme Electron Transfer in a Live Cell with Conducting Atomic Force Microscopy," *Anal Chem* 86, 7674-80 (2014).

21. Connelly, L. S. et al., "Graphene Nanopore Support System for Simultaneous High-Resolution AFM Imaging and Conductance Measurements," *ACS Appl Mater Inter* 6, 5290-96 (2014).

22. Meckes, B., Arce, F. T., Connelly, L. S., and Lal, R., "Insulated Conducting Cantilevered Nanotips and Two-Chamber Recording System for High Resolution Ion Sensing AFM," *Sci Rep* 4, 2045-22 (2014).

23. Abbou, J., Demaille, C., Druet, M. and Moiroux, J., "Fabrication of Submicrometer-Sized Gold Electrodes of Controlled Geometry for Scanning Electrochemical-Atomic Force Microscopy," *Anal Chem* 74, 6355-63 (2002).

24. Dobson, P. S., Weaver, J. M. R., Holder, M. N., Unwin, P. R. and Macpherson, J. V., "Characterization of Batch-Microfabricated Scanning Electrochemical-Atomic Force Microscopy Probes," *Anal Chem* 77, 424-34 (2005).

25. Kaemmer, S. B., "Introduction to Bruker's ScanAsyst and PeakForce Tapping AFM Technology," *Bruker Application Notes* 133, (2011).

26. Berquand, A., "Quantitative Imaging of Living Biological Samples by PeakForce QNM Atomic Force Microscopy," *Bruker Application Notes* 135, (2011).

27. Li, C., Minne, S., Pittenger, B. and Mednick, A., "Simultaneous Electrical and Mechanical Property Mapping at the Nanoscale with PeakForce TUNA," *Bruker Application Notes* 132, (2011).

28. Li, C. et al., "PeakForce Kelvin Probe Force Microscopy," *Bruker Application Notes* 140, (2013).

29. Huang, Z. et al., "Nanoscale Mapping of Permittivity and Conductivity with Scanning Microwave Impedance Microscopy," *Bruker Application Notes* 145, (2016).

30. Nellist, M. R. et al., "Atomic Force Microscopy with Nanoelectrode Tips for High Resolution Electrochemical, Nanoadhesion and Nanoelectrical Imaging," *Nanotechnology* 28, 095711 (2017).

31. Wain, A. J., Pollard, A. J. and Richter, C., "High-Resolution Electrochemical and Topographical Imaging Using Batch-Fabricated Cantilever Probes," *Anal Chem* 86, 5143-49 (2014).

32. Huang, Z. et al., "PeakForce Scanning Electrochemical Microscopy with Nanoelectrode Probes," *Microscopy Today* 24, 18-25 (2016).

33. Chen, Y. K., Sun, K., Audesirk, H., Xiang, C. X. and Lewis, N. S., "A Quantitative Analysis of the Efficiency of Solar-Driven Water-Splitting Device Designs Based on Tandem Photoabsorbers Patterned with Islands of Metallic Electrocatalysts," *Energ Environ* Sci 8, 1736-47 (2015).

34. Bard, A. J. and Faulkner, L. R., *Electrochemical Methods: Fundamentals and Applications*. 2nd Edition, (Wiley, 2000).

35. Jang, H. Y., Lee, S. K., Cho, S. H., Ahn, J. H. and Park, S., "Fabrication of Metallic Nanomesh: Pt Nano-Mesh as a Proof of Concept for Stretchable and Transparent Electrodes," *Chem Mater* 25, 3535-38 (2013).

36. Guo, C. F., Sun, T. Y., Liu, Q. H., Suo, Z. G. and Ren, Z. F., "Highly Stretchable and Transparent Nanomesh Electrodes Made by Grain Boundary Lithography," *Nat Commun* 5 (2014).

37. Walter, M. G. et al., "Solar Water Splitting Cells," *Chem Rev* 110, 6446-73 (2010).

38. Haynes, C. L. and Van Duyne, R. P., "Nanosphere Lithography: A Versatile Nanofabrication Tool for Studies of Size-Dependent Nanoparticle Optics," *J Phys Chem B* 105, 5599-11, (2001).

39. Wei, C., Bard, A. J. and Mirkin, M. V., "Scanning Electrochemical Microscopy 31. Application of SECM to the Study of Charge-Transfer Processes at the Liquid-Liquid Interface," *J Phys Chem* 99, 16033-42 (1995).

40. Love, J. C., Estroff, L. A., Kriebel, J. K., Nuzzo, R. G. and Whitesides, G. M., "Self-Assembled Monolayers of Thiolates on Metals as a Form of Nanotechnology," *Chem Rev* 105, 1103-69, (2005).

41. Patel, A. N. et al., "A New View of Electrochemistry at Highly Oriented Pyrolytic Graphite," *J Am Chem Soc* 134, 20117-30 (2012).

42. Zhang, G. H. et al., "Molecular Functionalization of Graphite Surfaces: Basal Plane versus Step Edge Electrochemical Activity," *J Am Chem Soc* 136, 11444-51 (2014).

43. Guell, A. G. et al., "Redox-Dependent Spatially Resolved Electrochemistry at Graphene and Graphite Step Edges," *ACS Nano* 9, 3558-71 (2015).

44. Schauermann, S., Nilius, N., Shaikhutdinov, S. and Freund, H. J., "Nanoparticles for Heterogeneous Catalysis: New Mechanistic Insights," *Accounts Chem Res* 46, 1673-81 (2013).

45. Xia, Y. N., Yang, H. and Campbell, C. T., "Nanoparticles for Catalysis," *Accounts Chem Res* 46, 1671-72 (2013).

46. Smith, W. A., Sharp, I. D., Strandwitz, N. C. and Bisquert, J., "Interfacial Band-Edge Energetics for Solar Fuels Production," *Energ Environ* Sci 8, 2851-62 (2015).

47. Nellist, M. R., Laskowski, F. A. L., Lin, F. D., Mills, T. J. and Boettcher, S. W., "Semiconductor-Electrocatalyst Interfaces: Theory, Experiment, and Applications in Photoelectrochemical Water Splitting," *Accounts Chem Res* 49, 733-40 (2016).

Authors

Zhuangqun Huang,[a] Peter De Wolf,[a] Chunzeng Li,[a] Rakesh Poddar,[a] Ivan Yermolenko,[a] Andreas Mark,[b] Sebastian Gödrich,[b] Christian Stelling,[b] Michael R. Nellist,[c] Yikai Chen,[d] Jingjing Jiang,[d] Jonathan R. Thompson,[d] Georg Papastavrou,[b] Markus Retsch,[b] Shannon W. Boettcher,[c] Chengxiang Xiang,[d] and Bruce S. Brunschwig[d]

[a] Bruker Nano Surfaces, 112 Robin Hill Road, Goleta, California, CA, 93117, USA
[b] Physical Chemistry, University of Bayreuth, Universitätsstrasse, 95440 Bayreuth, Germany
[c] Department of Chemistry and Biochemistry, University of Oregon, Eugene, Oregon 97403, United States
[d] Joint Center for Artificial Photosynthesis, California Institute of Technology, Pasadena, CA, 91106, USA

©2017 Bruker Corporation. All rights reserved. Bruker Corporation and all other trademarks are the property of their respective companies. AN147, Rev. A0.

Bruker Nano Surfaces Divison
Santa Barbara, CA · USA
productinfo@bruker.com

www.bruker.com/peakforce-secm